JOURNAL OF GEOPHYSICAL RESEARCH, VOL. 94, NO. B2, PAGES 1927–1934, FEBRUARY 10, 1989

Theory of Thermal Recovery From a Spherically Stimulated Hot Dry Rock Reservoir

DEREK ELSWORTH[1]

Department of Mineral Engineering, The Pennsylvania State University, University Park

A conceptual model is presented to describe thermal recovery from a semi-infinite hot dry rock (HDR) geothermal reservoir containing an equidimensional permeable zone. Transient behavior may be represented uniquely by five dimensionless parameters. Variation in production temperature T_D with time t_D is influenced by reservoir throughput Q_D thermal porosity Φ_D and depth ratio a/z. Of these, only throughput Q_D exercises significant control on transient performance, the parameter being directly proportional to reservoir circulation rate and inversely proportional to the effective radius of the stimulated zone. Steady production temperature T_D is indexed to throughput Q_D and depth ratio a/z, only. Steady production temperatures are always highest for a host medium bounded by a proximal constant temperature surface and lowest for an insulated boundary. Boundary effects are insignificant for reservoir burial depths up to an order of magnitude greater than the reservoir radius. A threshold behavior in time (t_DQ_D) is evident for very large reservoir throughput (Q_D). This bounding behavior describes, in dimensionless time, the maximum rate at which thermal depletion may occur. This state is evident for large dimensionless throughput magnitudes (Q_D) corresponding directly with high circulation rates within the reservoir. Predictions compare favorably with results from a 300-day circulation test at the Fenton Hill Geothermal Energy Site, New Mexico.

INTRODUCTION

Geothermal extraction from deep hot dry rock (HDR) is a feasible method of energy recovery for which the basic physical viability has been established through conceptual [*Harlow and Pracht*, 1972; *Smith*, 1975], economic [e.g., *Murphy et al.*, 1985], and prototypical [e.g., *Murphy*, 1982] studies. All potential schemes incorporate circulation of a heat exchanging fluid, at depth, through an enclosed and geologically heated volume of permeable rock mass. Thermal energy is later recovered from the recirculating fluid. Of crucial importance to the economic viability of any prototypical scheme are the requirements of minimal fluid loss, low flow impedance, and high and sustained thermal output.

The original concept for HDR thermal recovery involved the artificial stimulation of a permeable zone, at depth in an initially impermeable formation, by creation of a massive hydraulic fracture. Analogues have been presented that are capable of investigating thermal output histories of the resulting planar [*Lauwerier*, 1955; *Carslaw and Jaeger*, 1959; *Gringarten and Sauty*, 1975] or multiple parallel [*Gringarten and Witherspoon*, 1973; *Gringarten et al.*, 1975; *Bodvarsson and Tsang*, 1982; *Witherspoon et al.*, 1982] fracture geometries where deformational effects may also be incorporated [*Abe et al.*, 1979]. These model require that flow is confined in either single or multiple parallel fractures rather than dispersed within a confined volume of the rock mass. Recent evidence, however, in the attempted hydraulic fracturing of deep rocks containing a relic joint structure, indicates that a distinct stimulated volume may develop as opposed to the propagation of a single, essentially linear feature. This behavior has been reported at sites in the United Kingdom [*Pine and Batchelor*, 1984; *Baria et al.*, 1987] and the United States [*Fehler*, 1987].

The behavior is evidenced by both the scattered distribution of seismic sources at depth and the predominance of shear event signatures within the active microseismic cloud. Tracer testing [*Robinson and Tester*, 1984] supports the seismic record in determining the extent of porosity enhancement. Seismic activity is commonly evident during both stimulation and production phases of reservoir development. This may be attributed to the mixed and simultaneous development of fracture propagation processes including, thermal fatigue cracking, hydraulic jacking, and dilational bridging of remnant fracture planes, present at depth. Computational simulations incorporating fluid pressure transients [*Pine and Cundall*, 1985] and advective thermal transport transients [*Elsworth*, 1987; *Jianman*, 1988] have reproduced the behaviors of stimulated block jointed thermal reservoirs.

Artificial stimulation at depth may prove advantageous in extending useful reservoir life and maximizing energy production. The long and tortuous flow paths implicit within such a structure may, however, degrade net energy recovery as a result of the increased pumpage requirements necessitated by high flow impedance [*White*, 1982]. The interplay of these factors, among others, condition the economic feasibility of any project. Of critical interest in determining feasibility is the projected history of effluent fluid temperature, conditioned by prescribed flow rates, known (or surmised) reservoir geometry and dimension, and initial rock temperature at depth. A conceptual study is presented to examine the production histories of HDR geothermal reservoirs produced through a near equidimensional and finite volume zone of stimulation.

CONCEPTUAL MODEL

Thermal energy is withdrawn from the system through circulation of a fluid within a spherical and hydraulically closed zone of radius a. The secondary porosity of this zone is finite with the surrounding medium retaining zero secondary porosity. Fluid is circulated at constant volumetric flow rate

[1]Temporarily at Waterloo Centre for Groundwater Research, University of Waterloo, Waterloo, Ontario, Canada.

Paper number 88JB03852.
0148-0227/89/88JB-03852$05.00

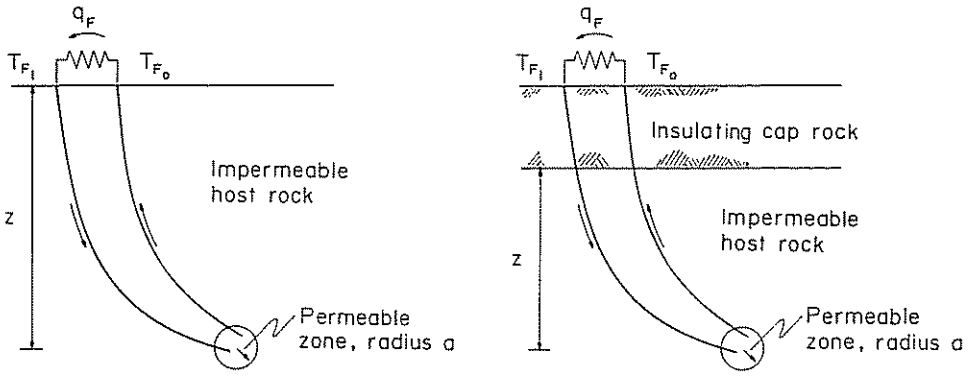

Fig. 1. Geometry of HDR geothermal energy recovery for semi-infinite reservoirs truncated by (left) constant temperature and (right) zero flux boundaries.

q_F with a prescribed injection temperature T_{F_i} and unknown outlet temperature T_{F_o}.

Model Assumptions

1. Fluid losses associated with temporal pressure changes and void volume increases are assumed negligible over the reservoir lifetime and are neglected. The radius of the stimulated zone remains static with production. Fluid expansion and buoyancy flow effects are neglected.

2. The temperature of the circulating fluid is raised, immediately upon injection, to the outlet temperature magnitude T_{F_o}. This requirement necessarily ignores any spatial dependence of fluid temperature within the permeable zone and therefore negates the development of any asymmetric component to the thermal drawdown in the surrounding medium. This assumption is warranted under circumstances where the thermal equilibration of individual rock blocks comprising the permeable zones is rapid relative to the transit time of the circulating fluid. Where primary interest is the gross (aggregated) magnitude of thermal energy production, rather than point determination of temperature distribution, the assumption is considered reasonable.

3. Thermal equilibrium between the percolating fluid and host rock is maintained at all times within the stimulated zone. The edge dimensions of individual rock blocks, delineated by active flow paths, are assumed sufficiently small that rapid equilibration will occur. The validity of this assumption may be tested with knowledge of t^{95}, the time to 95% equilibration following a change in surface temperature to any of the individual rock blocks. A spherical idealization of a cubic block, of edge dimension l, yields $t^{95} = 5.9 \times 10^{-2}\, l^2/\kappa$, where κ is the thermal diffusivity of the rock [*Elsworth*, 1987] denoted $\kappa = K_R/\rho_R c_R$, where K_R is thermal conductivity, ρ_R is density, and c_R is specific heat of the intact rock.

4. Thermal transport within the stimulated volume is purely advective. Pure conduction is the transport mechanism within the external medium.

5. The thermal capacities of the external rock $\rho_R c_R$, circulating fluid $\rho_F c_F$ and the permeable saturated zone $\rho_S c_S$, together with the thermal conductivity of the external rock K_R remain constant with time.

6. The influence of the natural geothermal gradient over the height of the stimulated zone is assumed negligible. This factor has been illustrated, in previous investigations, to be apparent only at small dimensionless times and is negligible for a realistic range of physical parameters [*Gringarten et al.*, 1975].

7. The domain containing the spherical permeable zone may be infinite or semi-infinite. The bounding layer of the half space may be retained at constant initial temperature or as a zero thermal flux (insulated) boundary. Geometries appropriate to these dual situations are illustrated in Figure 1.

8. The specific heat capacity of the spherical permeable zone is aggregated as $\rho_S c_S = (1 - \phi)\rho_R c_R + \phi \rho_F c_F$, where ϕ is the secondary porosity.

Energy Balance

The approach taken in the following is to define an energy balance relationship for the spherical permeable zone comprising the reservoir. The effect of thermal depletion in the surrounding host rock is introduced through a source term ($q_T(a, t)$) adding thermal energy to the central zone. The source term is obtained directly through analytical solution for a spherical source of constant strength in time. The combined system is then modified via linear superposition (Duhamel's theorem) to yield the transient behavior of the coupled interior (permeable zone) and exterior (host rock) problems incorporating circulation regulated thermal depletion.

Considering first the permeable zone to be supplied by a total thermal energy production rate $q_T(a, t)$ from the surrounding mass and to be depleted by the heat removed by fluid circulating at flow rate q_F, an energy balance equation may be written for the closed system as

$$q_T(a, t) = q_F \rho_F c_F (T_{F_o}(t) - T_{F_i}) + \frac{4}{3}\pi a^3 \rho_S c_S\, \partial T_{F_o}(t)/\partial t \qquad (1)$$

where T_{F_o} is the outlet fluid temperature from the permeable zone of radius a. Equation (1) requires that heat energy supplied to the permeable zone as a result of thermal drawdown in the surrounding medium (through q_T) is directly balanced by temperature changes in the spherical interior. The first and second terms on the right-hand side represent, respectively, the thermal energy removed from the system by the circulating fluid, and the thermal energy absorbed by the reservoir under a unit change in temperature. The magnitude of $q_T(a, t)$, representing the thermal flux supplied from the reservoir exterior, may be obtained by independently solving the spherically symmetric initial value problem as

$$\kappa\left[\frac{\partial^2 T_R(r, t)}{\partial r^2} + \frac{2}{r}\frac{\partial T_R(r, t)}{\partial r}\right] = \frac{\partial T_R(r, t)}{\partial t} \qquad (2)$$

where r is the radial coordinate. Boundary and initial con-

ditions are applied as

$$T_R(r, t) = T_R \qquad t \le 0^- \qquad a \le r \le \infty$$

$$T_R(a, t) = T_{F_o}(t) \qquad 0^+ \le t \le +\infty$$

$$T_R(\infty, t) = T_R \qquad -\infty \le t \le +\infty$$

where T_R is the initial rock temperature at the reservoir depth z and κ is the thermal diffusivity of the surrounding rock. Solution is available to (2) for a radial flux of constant magnitude with time given as $q_T(a, t)/4\pi a^2 = \text{constant}$ over the contour $r = a$ [*Carslaw and Jaeger*, 1959, p. 248] as

$$q_T(a, t) = 4\pi K_R r (T_R - T_{F_o}) \left\{ \operatorname{erfc} \frac{(r-a)}{2(\kappa t)^{1/2}} - \exp\left[\frac{(r-a)}{a} + \frac{\kappa t}{a^2}\right] \cdot \operatorname{erfc}\left[\frac{(r-a)}{2(\kappa t)^{1/2}} + \frac{(\kappa t)^{1/2}}{a}\right] \right\}^{-1} \tag{3}$$

Equation (3) represents the thermal energy supplied, through thermal drawdown in the impermeable host rock, to the embedded permeable zone. Therefore substitution of (3) directly into (1) and solution with time allows the outlet temperatures T_{F_o} to be determined for the coupled system comprising a central permeable zone embedded within an infinite surrounding medium. It should be cautioned, however, that since (3) is valid for a constant applied flux magnitude only, the previous substitution is insufficient to give the full temperature history of the coupled system since further accommodation of time-dependent boundary conditions is necessary.

Solution for the infinite case is a limiting form of the semi-infinite solution as dimensionless depth ratio a/z approaches zero. For this reason, only the latter will be developed in detail. The interested reader may determine that for large dimensionless reservoir depth ratios, as represented in Figure 1, or at small dimensionless times, the two behaviors converge.

The method of images is used to satisfy the zero flux or constant temperature boundary conditions desired at the half space boundary. Spherical sources of identical or opposite strengths are applied at a separation of $2z$. Since the radius of the sphere is considered finite, the influence of a second source on the temperature distribution surrounding the first will vary with connecting radius r_α as illustrated in Figure 2(top). To retain the problem at a tractable level, the temperature change induced on the surface of sphere A by a source at sphere B is area averaged and applied as a mean temperature defined as $T_B(r_\alpha) = \langle T_R - T_{F_o} \rangle_A$, as illustrated in Figure 2(bottom). Thus the mean temperature induced over the surface of sphere A by a source at B is given by the integral of $(T_R - T_{F_o})$ evaluated over the surface area of sphere A. With some rearrangement, this may be written as

$$\langle T_R - T_{F_o} \rangle_A = \frac{1}{2} \int_0^\pi (T_R - T_{F_o}(r_\alpha))_B \sin \alpha \, d\alpha \tag{4}$$

where the connecting radius identified in Figures 2(top) and 2(bottom) is given as

$$r_\alpha = 2z \left[1 + \left(\frac{a}{2z}\right)^2 - \frac{a}{z} \cos \alpha \right]^{1/2} \tag{5}$$

and subscript A refers to temperature change induced at sphere A.

Combining the influence of the two complementary or opposed sources at a separation $2z$ gives the aggregated thermal drawdown $\langle T_R - T_{F_o} \rangle$ on the permeter of sphere A under a

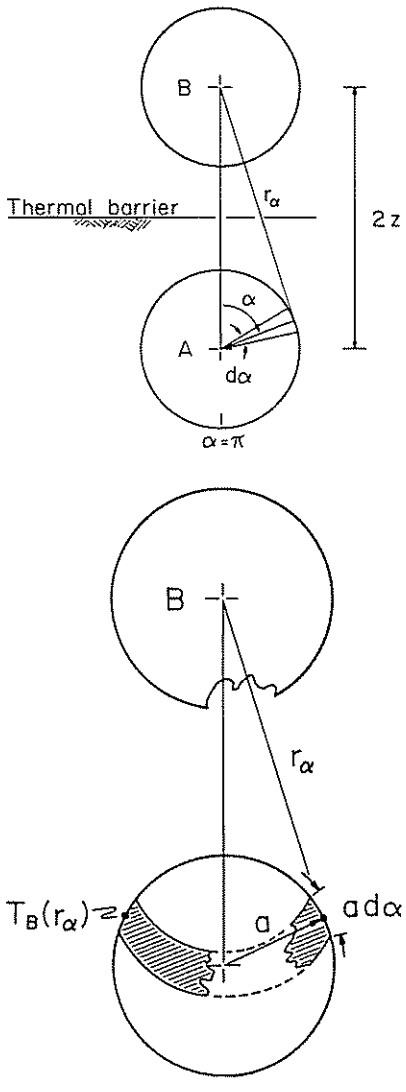

Fig. 2. Representation of semi-infinite extraction geometries. (Top) Definition of connecting radius r_α. (Bottom) Areal averaging of induced temperature T_B on sphere A.

constant extraction rate $q_T(a, t)_A$ as

$$q_T(a, t)_A = 4\pi K_R a \langle T_R - T_{F_o} \rangle \left[C_1 \pm \frac{1}{2} \int_0^\pi C_2 \sin \alpha \, d\alpha \right]^{-1} \tag{6}$$

where

$$C_1 = 1 - \exp\left(\frac{\kappa t}{a^2}\right) \operatorname{erfc} \frac{(\kappa t)^{1/2}}{a} \tag{7}$$

$$C_2 = \frac{a}{r_\alpha} \left\{ \operatorname{erfc} \frac{(r_\alpha - a)}{2(\kappa t)^{1/2}} - \exp\left[\frac{(r_\alpha - a)}{a} + \frac{\kappa t}{a^2}\right] \cdot \operatorname{erfc}\left[\frac{r_\alpha - a}{2(\kappa t)^{1/2}} + \frac{(\kappa t)^{1/2}}{a}\right] \right\} \tag{8}$$

and the positive and negative terminology of (6) refers to zero flux and constant temperature boundary conditions applied at the surface of the semi infinite medium, respectively. Where the zero flux condition is applied at the surface of the half space, the initial temperature distribution is assumed constant with depth and of magnitude T_R. For the constant surface temperature case a linear geothermal gradient is assumed of

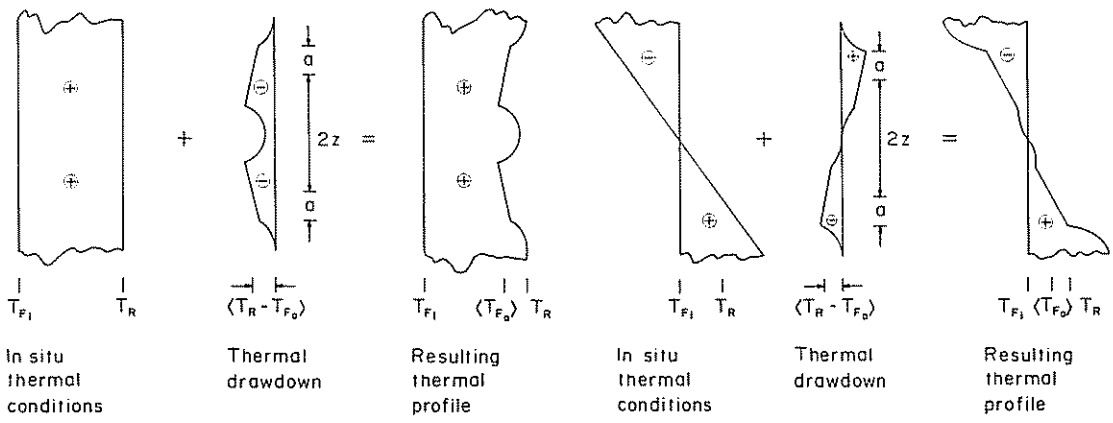

Fig. 3. Development of thermal profiles for (left) perfectly insulated and (right) constant temperature boundary conditions. From left, the components represent the initial in situ geothermal gradient, the thermal drawdown resulting from fluid circulation, and the resulting thermal profile.

ordinates T_{F_i} at the surface and magnitude T_R at the central depth of the reservoir, z. This clearly represents the case of a perfectly efficient heat exchanger at surface, capable of returning the effluent fluid, initially at temperature T_{F_o}, directly to the ambient surface air temperature. As illustrated in Figure 3, for finite reservoir radius a the solution may only be regarded as approximate. Locally, temperatures above the stimulated zone may fall below the inlet temperature T_{F_i}. This facet of the analysis is occasioned by requiring that thermal energy is withdrawn uniformly from the surface area of the spherical inclusion rather than applying strictly temperature controlled boundary conditions. It is not anticipated that significant error will result from this constraint.

Application of Duhamel's theorem [*Carslaw and Jaeger*, 1959, p. 30] to (6) allows thermal influx into the reservoir to be determined for a sequence of time variant temperature boundary conditions applied on the surface of the embedded sphere A as

$$q_T(a,t)_A = 4\pi K_R a \int_0^t \frac{\partial}{\partial t}\langle T_R - T_{F_o}\rangle \left[C_1 \pm \frac{1}{2}\int_0^\pi C_2 \sin\alpha\, d\alpha\right]^{-1} d\tau \tag{9}$$

where τ is the discrete parameter of integration ranging from time zero $\tau = 0$ to the current time level of interest $\tau = t$. Equation (9) represents the time-dependent thermal discharge to the perimeter of the spherical permeable zone under arbitrary time dependent thermal boundary conditions $\langle T_R - T_{F_o}\rangle$. Substitution of (9) into the energy balance of (1) and rearrangement as a finite difference expression in time, yields, for constant inlet temperature, T_{F_i}

$$\Delta T_{F_o}{}^1 \frac{1}{\Delta t}\int_{t_0}^{t_1} -[C_1 \pm \bar{C}_2]^{-1}\, d\tau + \Delta T_{F_o}{}^2 \frac{1}{\Delta t}\int_{t_1}^{t_2} -[C_1 \pm \bar{C}_2]\, d\tau + \cdots + \cdots + \Delta T_{F_o}{}^n \frac{1}{\Delta t}\int_{t_{n-1}}^{t_n} -[C_1 \pm \bar{C}_2]\, d\tau = \frac{q_F \rho_F c_F}{4\pi K_R a}\langle T_{F_o}{}^n - T_{F_i}\rangle + \frac{\rho_S c_S a^2}{3K_R \Delta t}\Delta T_{F_o}{}^n \tag{10}$$

where

$$\Delta T_{F_o}{}^n = T_{F_o}{}^n - T_{F_o}{}^{n-1} \tag{11}$$

$$\bar{C}_2 = \frac{1}{2}\int_0^\pi C_2 \sin\alpha\, d\alpha \tag{12}$$

and superscript n refers to the nth time level. A further initial condition must be supplied for solution. Fluid in the stimulated zone is initially in thermal equilibrium with the surrounding rock. Thus $T_{F_o}(0) = T_R(a, 0)$. The temporal integrations must be completed numerically where the expressions for C_1 and C_2 in (7) and (8) are discretely replaced in time by

$$C_1 = 1 - \exp\left[\frac{\kappa(t_n - \tau)}{a^2}\right]\operatorname{erfc}\left[\frac{\kappa(t_n - \tau)}{a}\right]^{1/2} \tag{13}$$

$$C_2 = \frac{a}{r_x}\left\{\operatorname{erfc}\left[\frac{(r_x - a)}{2(\kappa(t_n - \tau))^{1/2}}\right] - \exp\left[\frac{(r_x - a)}{a} + \frac{\kappa(t_n - \tau)}{a^2}\right] \cdot \operatorname{erfc}\left[\frac{(r_x - a)}{2(\kappa(t_n - \tau))^{1/2}} + \frac{(\kappa(t_n - \tau))^{1/2}}{a}\right]\right\} \tag{14}$$

where τ is the discrete parameter of integration. In the following, three point quadrature is used to evaluate the time integral for finite a/z. Where $a/z \to 0$ then $\bar{C}_2 \to 0$ and the discrete time integral may be represented in closed form at current time level t_n as

$$\int_{t_0}^{t_1} -C_1{}^{-1}\, d\tau = \left[\tau - \frac{2a(t_n - \tau)^{1/2}}{(\pi\kappa)^{1/2}}\right]_{t_0}^{t_1} \tag{15}$$

Solution to the final energy balance identified in (10) is evaluated numerically and represented uniquely in terms of the dimensionless groups

$$\frac{\langle T_{F_i} - T_{F_o}\rangle}{(T_{F_i} - T_R)} = \mathscr{F}\left(\frac{q_F \rho_F c_F}{K_R a}; \frac{K_R t}{\rho_R c_R a^2}; \frac{\rho_S c_S}{\rho_R c_R}; \frac{a}{z}\right) \tag{16}$$

or, in shorthand,

$$T_D = \mathscr{F}\left(Q_D; t_D; \Phi_D; \frac{a}{z}\right)$$

where $\mathscr{F}(\ \ )$ merely records the functional dependence of the parameters.

Physically, these groups may be denoted as dimensionless output temperature T_D, dimensionless reservoir throughput Q_D, dimensionless time t_D, dimensionless heat capacity or porosity Φ_D, and dimensionless depth (a/z).

Steady Condition

Although intractable analytically for the transient case, (10) may be evaluated for the long term. Noting that as $t \to \infty$

$$C_1 \rightarrow 1 \qquad C_2 \rightarrow \frac{a}{r} \tag{17}$$

$$\bar{C}_1 \rightarrow \frac{1}{2}\int_0^{\pi} \frac{a}{r_z} \sin\alpha \, d\alpha = \frac{a}{2z} \tag{18}$$

Substitution of (17) and (18) into (6) and the result into (1) gives, following some manipulation, the steady condition as

$$\frac{\langle T_{F_i} - T_{F_o} \rangle}{(T_{F_i} - T_R)} = \left[1 + \frac{q_F \rho_F c_F}{4\pi K_R a}\left(1 \pm \frac{a}{2z}\right)\right]^{-1} \tag{19}$$

with the positive and negative signatures of the dimensionless depth term referring to cases of zero flux and constant temperature constraints on the surface of the half space, respectively.

These results are significant, since they predict finite thermal recovery at large dimensionless times. This is consistent with steady results obtained for the characterization of spherically symmetric magma bodies at depth [*Hardee and Lawson*, 1980]. This facet of the conceptual model is perhaps more realistic than those predicting $T_D = 0$ for all Q_D at large dimensionless times. Of significance in the steady condition is that the long term production temperature is lower for the case of an insulated caprock than for that of a caprock retained at constant temperature. This result appears intuitively reasonable given that the insulated geometry is able to deplete the thermal regime in a semi-infinite volume rather than an infinite volume.

Results and Discussion

Reservoir performance may be defined in terms of the five dimensionless parameters T_D, t_D, Q_D, Φ_D, and a/z. Of prime interest in determining the projected longevity of energy production is knowledge of the reduction in reservoir production temperature T_D as a function of dimensionless time t_D for different production or pumping rates Q_D. The results may be presented compactly if thermal drawdown T_D is recorded relative to the product $t_D Q_D$ as utilized in the following. Terms representing reservoir porosity Φ_D and reservoir depth a/z also impact the resulting energy production histories and must be examined to determine the sensitivity of the solution to their change.

For igneous rocks the thermal porosity term Φ_D will always be greater than unity. Physical constants representative of granite as the host and water as the percolating fluid impart $\Phi_D \cong 1.1$ for an unrealistically high secondary porosity of 10%. As secondary porosity is reduced ($\phi \rightarrow 0$) the dimensionless reservoir porosity term approaches unity. A suitable range for the reservoir porosity parameter would therefore appear to be $1.0 \leq Q_D \leq 1.1$.

Results for temperature histories in an infinite medium ($a/z = 0$) are reported in Figure 4. As a natural consequence the solution exhibits uniform rock temperature at the periphery of the permeable zone. It is apparent that thermal history is sensitive to Φ_D only for large dimensionless throughputs Q_D. For $Q_D < 10^1$ the results are indistinguishable for the two thermal porosities Φ_D of 1.0 and 1.1. Even for large Q_D values the discrepancy appears insignificant. The sense of the modification to the thermal histories suggests that increased porosities slightly forestall thermal depletion. As evidenced in (19) and also in Figure 4, long-term (steady) withdrawal temperatures remain finite and, more importantly, significant for throughput values Q_D less than 10^3. Depending on the threshold temperatures required to ensure efficient energy conversion, the productive life of the geothermal reservoir may remain unbounded.

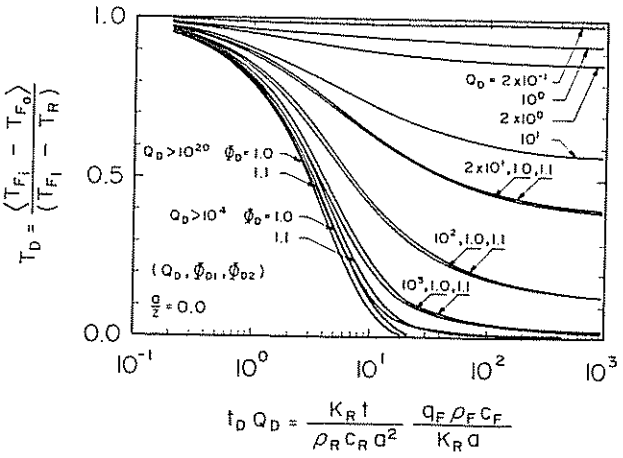

Fig. 4. Variation in dimensionless output temperature T_D with dimensionless time $t_D Q_D$ for a permeable zone within an infinite medium. Labels refer to dimensionless throughput Q_D, thermal porosity Φ_{D1} for $\Phi_D = 1.0$, and thermal porosity Φ_{D2} for $\Phi_D = 1.1$.

For very large magnitudes of Q_D, a threshold behavior is apparent. Figure 4 illustrates the predicted temperature history as $Q_D \rightarrow \infty$. This behavior corresponds to high circulation rates where the thermal supply form the surrounding rock becomes negligible. In this instance, solution of (1) with $q_T(a, t) = 0$ gives $T_D = \exp[-3t_D Q_D/4\pi]$ resulting in the limiting curvature in Figure 4 for $Q_D = 10^{20}$. Physically, the limiting behavior corresponds to thermal drawdown in a sphere of radius a, embedded within an insulating medium. The total thermal energy extracted at full depletion is given by the product of sphere volume, specific heat capacity of that volume, and temperature change. For fixed thermal diffusivities of the host medium, together with a constant reservoir dimension a, the thermal histories are moved laterally (earlier) in real time by one order of magnitude for every increase in real circulation rate q_F of one order of magnitude. Thus as anticipated, the energy production rate is directly conditioned by the circulation rate through the system. Intuitively, minimal thermal depletion is evident in Figure 4 for small flow rates q_F or large reservoir diameters as evidenced by small values of dimensionless throughput Q_D.

The thermal response of semi-infinite systems are bounded, in the most extreme case, by a depth ratio a/z of unity. Although results are physically meaningless for the instance of a constant temperature surface, comparisons are useful, since thermal histories bound candidate responses for all depth ratios between unity and zero. Semi-infinite responses are illustrated in Figure 5 for a depth ratio of unity. The influence of an insulated surface is to reduce the ultimate steady outlet temperature T_D over that of the infinite case. This result appears reasonable since a reduced volume, and hence (reduced) thermal reservoir, is available for depletion in the semi-infinite case. Conversely, the presence of a surface retained at constant (ambient) temperature elicits a more favorable (hotter) thermal response to that of the infinite case. The influence of boundaries is only significant for intermediate values of dimensionless throughput Q_D and, even in these instances is only apparent at large dimensionless times $t_D Q_D$. The range $10^{-1} < Q_D < 10^3$ brackets this boundary sensitive region. The branching of thermal histories occurs earlier in dimensionless time with decreasing throughput Q_D.

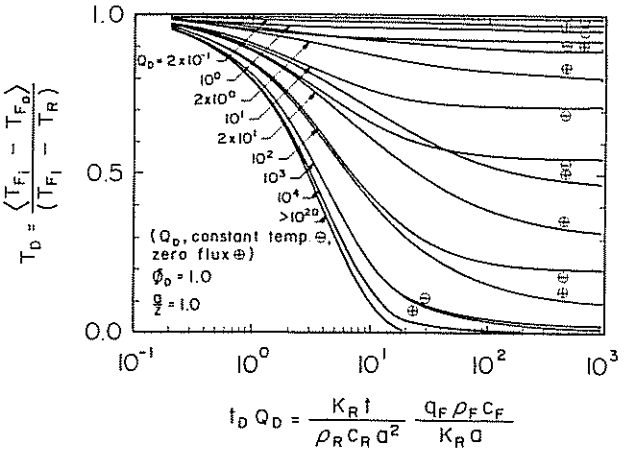

Fig. 5. Variation in dimensionless output temperature T_D with dimensionless time $t_D Q_D$ for a permeable zone at depth $a/z = 1.0$. Labels refer to dimensionless throughput Q_D, constant temperature boundary (minuses), and zero flux boundary (pluses).

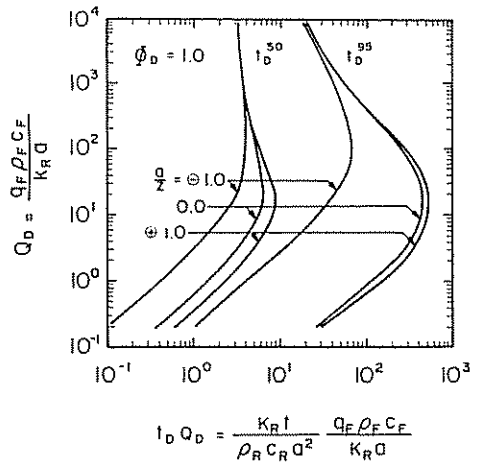

Fig. 7. Variation in 50% t_D^{50} and 95% t_D^{95} depletion times with dimensionless throughput Q_D for thermal porosity $\Phi_D = 1.0$. Results shown for constant temperature (minus) and zero flux (plus) boundaries.

Thermal responses for depth ratios of one half are illustrated in Figure 6. Similar to the results for $a/z = 1$, the influence of boundaries are only significant in the range $10^{-1} < Q_D < 10^3$. As the reservoir depth ratio a/z decreases to 10^{-1}, the results for bounded reservoirs are indistinguishable from the infinite case and may be correctly interpolated from Figure 4.

From knowledge of thermal response, depletion times may be directly determined to aid in defining useful lifetimes of individual reservoir configurations. Ultimate withdrawal temperatures may be determined from (19). The time required for the outlet temperature to each 50 and 95% of the steady temperature values are defined as $t_D{}^{50}Q_D$ and $t_D{}^{95}Q_D$, respectively. These results are illustrated in Figure 7 for the limiting cases of bounded and infinite reservoir geometries for all significant values of Q_D. Reservoirs bounded by a constant temperature surface deplete more rapidly than either insulated or infinite geometries. This behavior is most marked in the very long term performance as evidenced by the $t_D{}^{95}Q_D$ parameter.

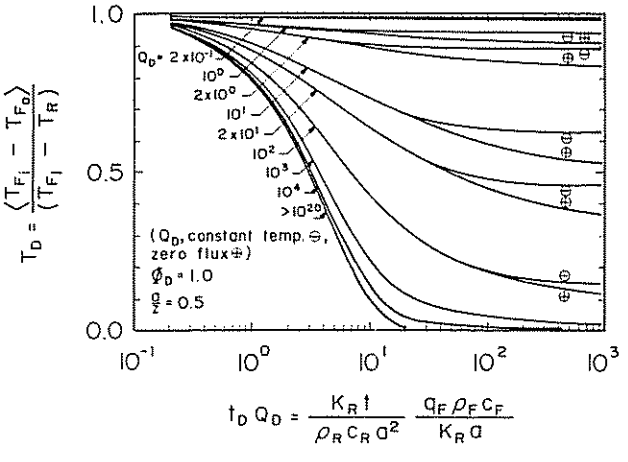

Fig. 6. Variation in dimensionless output temperature T_D with dimensionless time $t_D Q_D$ for a permeable zone at depth $a/z = 0.5$. Labels refer to dimensionless throughput Q_D, constant temperature boundary (minuses), and zero flux boundary (pluses).

FENTON HILL HDR RESERVOIR

Comparison is possible between predictions elicited from the thermal recovery model and results from a 300-day circulation test conducted at the Fenton Hill experimental reservoir in New Mexico. Results are reported from run segment 5 of experiment 217 in the work by *Zyvoloski et al.* [1981] where long-term circulation was induced between the injection level at 2903 m and withdrawal level at 2708 m below surface. The known separation of the injection and withdrawal points together with available seismic data suggest a permeable zone or reservoir diameter of the order of 200 m. Appropriate material and site parameters are documented in Table 1. The least well-defined of the required input parameters is the dimension of the permeable zone. An estimated radius of $a = 100$ m yields a dimensionless throughput of $Q_D = 93$ when the parameters of Table 1 are utilized directly. Predicted thermal drawdowns are reported in Figure 8 in real time for dimensionless throughputs spanning 50–150. These magnitudes correspond to reservoir radii of 186 m to 62 m and show some correspondence with the data recovered from the 300-day circulation test. This correspondence is encouraging given the reasonableness of the physical parameters utilized in the comparison, however, the test duration is too brief to yield a conclusive comparison. Furthermore, the initial response is most strongly conditioned by thermal depletion of the immediate permeable zone. Only later in the drawdown history will the influence of external heat supply, from around the spherical zone, become apparent.

If, from the data of Figure 8, a dimensionless throughput Q_D of 100 is assumed reasonable for this physical system, the full thermal drawdown history may be determined directly from Figure 4. The dimensionless time axis ($t_D Q_D$) may be converted to real time by requiring that $a = 100$ m. The time axis then spans from 10^2 days (0.27 years) on the left-hand side to 10^6 days (2740 years) on the right-hand side allowing the full thermal depletion history, and consequently, the productive lifetime and output during this lifetime, to be projected.

TABLE 1. Physical Properties, Run Segment 5

Parameter	Magnitude	Units	Source
Rock thermal diffusivity κ	1.1×10^{-6}	$m^2\ s^{-1}$	*Kruger* [1982]
Rock thermal conductivity K_R	2.71	$J\ s^{-1}\ m^{-1}\ °C^{-1}$	*Kruger* [1982]
Water specific heat capacity $\rho_F c_F$	4.19×10^6	$J\ m^{-3}\ °C^{-1}$	*Bennett and Myers* [1982]
Injection temperature T_{F_i}	25	°C	*Zyvoloski et al.* [1981]
Initial in situ temperature T_R	197	°C	*Zyvoloski et al.* [1981]
Circulation rate q_F	6×10^{-3}	$m^3\ s^{-1}$	*Zyvoloski et al.* [1981]

CONCLUSIONS

A simple but meaningful mathematical model is presented to represent the transient behavior of HDR geothermal energy systems. The following conclusions may be drawn.

1. The performance of the system appears insensitive to reservoir burial depth or the proximity of thermal barriers. Rather, behavior is conditioned directly by the preproduction rock temperature T_R in the location of the zone of stimulation.

2. For a defined magnitude of dimensionless throughput Q_D, variations in reservoir thermal porosity, represented through the term Φ_D, affects fluid production temperatures T_D minimally. For $\Phi_D = 1.1$, representative of a granite of approximately 10% secondary porosity, the influence is observable only for small dimensionless throughput values $Q_D < 10^2$. However, since the fluid circulation rate q_F is strongly controlled by changes in secondary porosity, it is misleading to view the effect of Φ_D in isolation. Small increases in Φ_D may disproportionately increase circulation rates and, thereby, alter (increase) the appropriate magnitude of dimensionless throughput Q_D.

3. Significant steady heat production rates are established for all dimensionless throughputs Q_D greater than 10^3. The long-term dimensionless temperature T_D is indexed through the dimensionless variables of throughput Q_D and depth ratio a/z, only. Higher steady production temperatures are recovered for low circulation rates q_F or large reservoir radii a.

4. For large dimensionless throughputs Q_D, corresponding to large circulation rates q_F or small reservoir radii a, a threshold behavior is evident. This bounding behavior describes, in terms of dimensionless time ($t_D Q_D$), the maximum rate at which thermal depletion may occur. This threshold state is indexed directly to dimensionless throughput Q_D and is apparent for $Q_D < 10^3$.

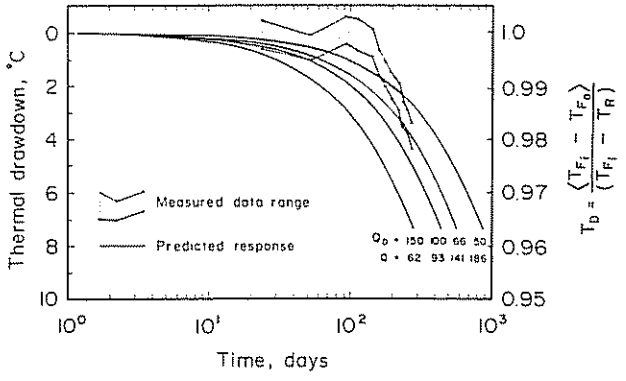

Fig. 8. Thermal response of the Fenton Hill 300-day circulation test [*Zyvoloski et al.*, 1981]. Data spread represents performance measured relative to the initial mean reservoir temperature or the highest mean reservoir temperature. Reservoir radii (a) are in meters.

5. Large radii or low circulation throughput systems have the most desirable thermal recovery characteristics in the long term. This behavior is further conditioned, however, by flow impedence characteristics of the reservoir and cannot therefore be viewed in isolation.

NOTATION

a radius of permeable zone, m.
a/z depth ratio, dimensionless.
c_F specific heat of circulating fluid, $J\ kg^{-1}\ K^{-1}$.
c_R specific heat of rock outside the permeable zone, $J\ kg^{-1}\ K^{-1}$.
c_S specific heat of saturated rock within the permeable zone of secondary porosity ϕ, $J\ kg^{-1}\ K^{-1}$.
K_R thermal conductivity of rock outside the permeable zone, $W\ m^{-1}\ K^{-1}$.
q_F fluid circulation rate, m^3/s.
$q_T(a, t)$ total thermal energy production rate resulting from a single spherical source, J/s.
$q_T(a, t)_A$ total aggregated thermal energy production rate on the surface of spherical source A resulting from real source A and image source B at separation $2z$, J/s.
Q_D reservoir throughput, dimensionless.
r radius of interest, m.
r_z radius from the center of image source B to the surface of source A (see Figure 2(top)) m.
l fracture spacing within permeable zone, m.
t time, s.
t^{95} time to 95% thermal equilibration for a single, fracture delimited, rock cube, s.
t_D time, dimensionless.
t_n time at the nth level, s.
T_D fluid temperature (influent versus effluent differential) at withdrawal, dimensionless.
T_{F_i} influent fluid temperature, K.
$T_{F_o}(t)$ effluent fluid temperature, K.
$\Delta T_{F_o}{}^n$ change in effluent temperature at time step n, K.
$T_R(r, t)$ rock temperature outside the permeable zone, K.
$\langle T_R - T_{F_o} \rangle_A$ spatially averaged temperature differential on the surface of the permeable zone, K.
z depth of reservoir burial below surface or cap rock, m.
α polar angle below vertical (see Figure 2(top)) degrees.
ϕ secondary porosity of peremeable zone, dimensionless.
Φ_D specific heat capacity ratio of saturated permeable zone of host rock, dimensionless.
κ thermal diffusivity of host rock, m^2/s.

ρ_F density of circulating fluid, kg/m^3.
ρ_R density of rock outside the permeable zone, kg/m^3.
ρ_S density of saturated rock within the permeable zone of secondary porosity ϕ, kg/m^3.
τ time integration parameter, s.

Acknowledgments. This material is based on work supported by the National Science Foundation under grant MSM-8708976. The assistance of Steven Birdsell, Michael Fehler, and Bruce Robinson in providing data from the Fenton Hill reservoir is greatly appreciated.

REFERENCES

Abe, H., L. M. Keer, and T. Mura, Theoretical study of hydraulically fractured penny-shaped cracks in hot, dry rocks, *Int. J. Numer. Anal. Meth. Geomech.*, *3*, 79–96, 1979.

Baria, R., A. S. P. Green, and R. H. Jones, Anomalous seismic events observed at the CSM HDR Project, *Rep. EUR 11164/1*, pp. 321–336, Comm. of European Commun., Brussels, 1987.

Bennett, C. O., and J. E. Meyers, *Momentum, Heat and Mass Transfer*, 3rd ed., McGraw-Hill, New York, 1982.

Bodvarsson, G. S., and C. F. Tsang, Injection thermal breakthrough in fractured geothermal reservoirs, *J. Geophys. Res.*, *87*(B2), 1031–1048, 1982.

Carslaw, H. S., and J. C. Jaeger, *Conduction of Heat in Solids*, 2nd ed., Clarendon, Oxford, 1959.

Elsworth, D., Thermal permeability enhancement of blocky rocks: Plane and radial flow, *Rep. EUR 11164/2*, pp. 235–273, Comm. of European Commun., Brussels, 1987.

Fehler, M. C., Stress control of seismicity patterns observed during hydraulic fracturing experiments at the Fenton Hill Hot Dry Rock Geothermal Energy Site, New Mexico, *Rep. EUR 11164/1*, pp. 299–319, Comm. of European Commun., Brussels, 1987.

Gringarten, A. C., and J. P. Sauty, A theoretical study of heat extraction from aquifers with uniform regional flow, *J. Geophys. Res.*, *80*(35), 6956–6962, 1975.

Gringarten, A. C., and P. A. Witherspoon, Extraction of heat from multiple fractured dry hot rock, *Geothermics*, *2*(3/4), 119–122, 1973.

Gringarten, A. C., P. A. Witherspoon, and Y. Ohnishi, Theory of heat extraction from fractured hot dry rock, *J. Geophys. Res.*, *80*(8), 1120–1124, 1975.

Hardee, H. C., and D. W. Larson, Thermal techniques for characterizing magma body geometries, *Geothermics*, *9*, 237–249, 1980.

Harlow, F. H., and W. E. Pracht, A theoretical study of geothermal energy extraction, *J. Geophys. Res.*, *77*, 7038, 1972.

Jiannan, X., A model for thermal permeability enhancement in low-temperature geothermal reservoirs, M.S. thesis, Pa. State Univ., University Park, 1988.

Kruger, P., Experimental studies on heat extraction from fractured geothermal reservoirs, in *Proceedings, First Japan-U.S. Joint Seminar on Hydraulic Fracturing and Geothermal Energy*, Martinus Nijhoff, The Netherlands, 1982.

Lauwerier, H. A., The transport of heat in an oil layer caused by the injection of hot fluid, *Appl. Sci. Res., Sect. A*, *5*, 145, 1955.

Murphy, H., Hot dry rock reservoir development and testing in the U.S.A., in *Proceedings, First Japan-U.S. Joint Seminar on Hydraulic Fracturing and Geothermal Energy*, pp. 33–58, Matinus Nijhoff, The Netherlands, 1982.

Murphy, H., R. Drake, J. Tester, and G. Zyvoloski, Economics of a conceptual 75 MW hot dry rock geothermal electric power-station, *Geothermics*, *14*(2/3), 459–474, 1985.

Pine, R. J., and A. S. Batchelor, Downward migration of shearing in jointed rock during hydraulic injections, *Int. J. Rock Mech. Min. Sci. 21*(5), 249–263, 1984.

Pine, R. J., and P. A. Cundall, Application of the fluid-rock interaction program (FRIP) to the modeling of hot dry rock geothermal energy systems, in *Proc. ISRM Symp. on Fundamentals of Rock Joints*, edited by O. Stephansson, pp. 293–302, Centek, Bjorkliedien, Sweden, 1985.

Robinson, B. A., and J. W. Tester, Dispersed fluid flow in fractured reservoirs: An analysis of tracer determined residence time distributions, *J. Geophys. Res.*, *89*(B12), 10,374–10,384, 1984.

Smith, M. C., The Los Alamos Scientific Laboratory dry hot rock geothermal project (LASL Group Q-22), *Geothermics*, *4*(1–4), 27–39, 1975.

White, A. A. L., Maximum tolerable reservoir impedances for hot dry rock, *Geothermics*, *11*(2), 121–130, 1982.

Witherspoon, P. A., G. S. Bodvarsson, K. Pruess, and C. F. Tsang, Energy recovery by water injection, *Spec. Rep. 12*, pp. 35–44, Geothermal Resour. Counc., Davis, Calif., 1982.

Zyvoloski, G. A., et al., Evaluation of the second hot dry rock geothermal reservoir: Results of phase I, run segment 5, *Rep. LA-8940-HDR*, pp. 94, Los Alamos Scientific Lab., Los Alamos, N. M., 1981.

D. Elsworth, Department of Mineral Engineering, 119 Mineral Sciences Building, The Pennsylvania State University, University Park, PA 16802.

(Received March 7, 1988;
revised September 20, 1988;
accepted October 10, 1988.)